Observed Lagrangian Transition of Stratocumulus into Cumulus during ASTEX: Mean State and Turbulence Structure

STEPHAN R. DE ROODE AND PETER G. DUYNKERKE

Institute for Marine and Atmospheric Research Utrecht, Utrecht University, Utrecht, the Netherlands

(Manuscript received 30 April 1996, in final form 21 November 1996)

ABSTRACT

Aircraft measurements made during the ''First Lagrangian'' of the Atlantic Stratocumulus Transition Experiment (ASTEX) between 12 and 14 June 1992 are presented. During this Lagrangian experiment an air mass was followed that was advected southward by the mean wind. Five aircraft flights were undertaken to observe the transition of a stratocumulus cloud deck to thin and broken stratocumulus clouds penetrated by cumulus from below. From the horizontal aircraft legs the boundary layer mean structure, microphysics, turbulence structure, and entrainment were analyzed. The vertical profiles of the vertical velocity skewness are shown to illustrate the transition of a cloudy boundary layer predominantly driven by longwave radiative cooling at the cloud top to one driven mainly by convection due to an unstable surface stratification and cumulus clouds. During the last flight before the stratocumulus deck was observed to be broken and replaced by cumuli, the total water flux, the virtual potential temperature flux, and the vertical velocity variance in the stratocumulus cloud layer were found significantly larger compared with the previous flights. To analyze the cloud-top stability the mean jumps of conserved variables across the inversion were determined from porpoising runs through the cloud top. These jumps were compared with cloud-top entrainment instability criteria discussed in the literature. It is suggested that enhanced entrainment of dry air is a key mechanism in the stratocumulus–cumulus transition.

1. Introduction

Stratocumulus-topped boundary layers (BL) are currently of great interest in many fields of meteorology. Due to its large horizontal extent, persistence, and high albedo stratocumulus influences the earth's energy balance and climate and is therefore important for global climate modeling. In order to understand the dynamics of such a cloud deck aircraft observations are used to interpret boundary layer properties like microphysics and turbulence. Experiments of this kind described by Brost et al. (1982a,b), Caughey and Kitchen (1984), Duynkerke et al. (1995), Nicholls (1984, 1989), and Nicholls and Leighton (1986) revealed that an important source for the generation of turbulent kinetic energy (TKE) is the longwave radiative loss at the top of the cloud. This leads to the formation of cold downdrafts that cause a positive buoyancy flux and drive the turbulence (Nicholls 1989). Another cloud-top process that is crucial in the evolution of the stratocumulus deck is the mixing of relatively warm and dry inversion air into the BL, a mechanism referred to as entrainment. Some aircraft measurements suggest that the entrainment rate in cloud-topped boundary layers is about an order of magnitude larger than in the dry convective BL (Nicholls and Turton 1986; Duynkerke et al. 1995), whereas smaller values were found by Kawa and Pearson (1989). When relatively warm and dry air from above the inversion is entrained into the cloudy BL, the temperature of the mixed parcels will be reduced due to the evaporation of cloud droplets. When the virtual potential temperature of the mixed parcel becomes lower than that of the cloudy environment, the parcel will descend, generating TKE and leading to more entrainment. This positive feedback mechanism, which may cause a rapid dissipation of the stratocumulus cloud deck, is referred to as cloud-top entrainment instability (CTEI). At present, an exact formulation of a CTEI criterion is still being discussed (Randall 1980; Deardorff 1980; Kuo and Schubert 1988; MacVean and Mason 1990; Siems and Bretherton 1992; Duynkerke 1993). Furthermore, latent and sensible heat fluxes from the surface, solar absorption in the cloud layer and subsequent decoupling, drizzle, and possible evaporation of droplets below the cloud deck influence the BL state.

Many papers in which aircraft measurements are described have concentrated on studying the relationship between the local structure and the local mean conditions rather than on investigating the evolution of the cloudy BL with time. The Atlantic Stratocumulus Transition Experiment (ASTEX) was set up in order to characterize the evolution and vertical structure of a marine

Corresponding author address: Dr. Stephan R. de Roode, IMAU, Utrecht University, Princetonplein 5, 3584 CC Utrecht, the Netherlands.
E-mail: S.R.deRoode@fys.ruu.nl

boundary layer (Albrecht et al. 1994). In ASTEX a very successful experiment was carried out during the ''First Lagrangian,'' in which an air mass was followed for two days. It was advected by the mean wind over a sea surface with increasing temperature. As a result, a solid stratocumulus deck gradually dissipated into thin and broken patches, which were penetrated from below by cumulus clouds (Roode and Duynkerke 1996; Martin et al. 1995; Wang and Lenschow 1995). These studies demonstrated that cumulus clouds are important for the hydrological cycle in that they supply the broken stratocumuli at the top of the boundary layer with moisture from the subcloud layer.

An elaborate description of the Lagrangian philosophy, synoptic setting, evolution of the mean state, and entrainment can be found in Bretherton and Pincus (1995) and Bretherton et al. (1995, hereafter referred to as BAS). For these studies vertical aircraft profiles were used to investigate the mean state of the boundary layer, ECMWF data were used to derive the subsidence, and bulk formulae were applied to determine the surface fluxes. In contrast, here we use measurements mainly from the horizontal legs and porpoise runs. As such, we analyze the turbulence structure from eddy correlation, and we focus on cloud-top stability and entrainment rates.

2. The first ASTEX Lagrangian

a. General description

The first ASTEX Lagrangian took place from 12 to 14 June 1992. Five flights were undertaken during this period, which were used for the study presented in this paper. These data were collected by the NCAR Electra (Flights RF05, RF06, and RF07) and two flights by the Meteorological Research Flight (MRF) C-130 aircraft (Flights A209 and A210) (see Table 1). Also, the University of Washington C-131 aircraft participated in the First Lagrangian, which measured cloud physics and chemistry. For the sake of readability we will use the notation Flights 1–5 for RF05, A209, RF06, RF07, and A210, respectively. The measurement strategy was chosen according to the Lagrangian philosophy (see Bretherton and Pincus 1995): all flights were performed in approximately the same air mass that was being advected southward by the mean wind.

A satellite observation made at 0900 UTC 12 June 1992 shows an extended area of stratocumulus clouds centered at about 39°N, 24°W(see Fig. 1a). At the eastern edge the cloud deck becomes less solid and the cloud structure more coarse, revealing cellular patterns with diameters of several tenths of kilometers. A very patchy cloud pattern becomes even more obvious 48 hours later, when it extends over an area of several hundreds of square kilometers (see Fig. 1b) and was encountered during Flight 5. Because of problems with the balloons released in order to follow the air mass trajectory, there is doubt about the exact location of the air mass for Flight 5. However, it is clear from Fig. 1b that any deviation of the aircraft from the real position of the air mass would not lead to a very different type of cloud. Hence we assume that the results of Flight 5 can be taken as being representative for a larger area.

During the First Lagrangian the boundary layer deepened with moderate to high wind speeds and substantial drizzle. The cloud developed from a solid stratocumulus layer to a layer filled with cumulus clouds penetrating the thin and broken stratocumulus above. Drizzle occurred on all flights. The sea surface temperature (SST) was measured directly by a radiometer aboard the aircraft. Along the trajectory the SST increased from 16.8 ($\pm$0.5)° to 21.1 ($\pm$0.3)°C. The inversion height and cloud thickness during the first three flights are quite stationary with values of about 750 and 500 m, respectively. The cumulus clouds observed on Flight 5 had a base at 500 m and a cloud top at 1600 m.

b. Cloud structure

A schematic picture of the cloud structure during the First Lagrangian described below is shown in Fig. 2.

1) FLIGHT 1

According to meteorological observations from the aircraft, the cloud deck consisted of a complicated two-layer structure. Sometimes scud clouds were observed in the lower layer, but some very small cumuli and foggy patches were seen as well. There was sporadic drizzle. The cloud base and top structure varied with location and time, and sometimes showed wavelike patterns but was sometimes found uniform. This flight started in the late afternoon (1719 UTC).

2) FLIGHT 2

During this night flight the drizzle rate below cloud base was considerable. There were no cumulus clouds under the stratocumulus deck.

3) FLIGHT 3

This flight was performed after Flight 2 ended. During Flight 3 the cloud structure became less homogeneous. Occasional showers were observed and cumulus clouds developed beneath the stratocumulus deck. The stratocumulus deck became thinner with time, possibly as a result of solar absorption, which became increasingly important during the second part of the flight.

4) FLIGHT 4

This flight started during the late afternoon and ended around sunset. The cumulus activity increased. During the flight some cumulus clouds were observed to pen-

TABLE 1. Details of cases studied.

Flight	Date	Location Start End	Time Start End (UTC)	Cloud top base (m)	Mean wind direction/speed $\Delta u/\Delta v$ (m s^{-1})	θ_e $\Delta\theta_e$ (K)	q_t Δq_t (g kg^{-1})	$\Delta\theta_v$ (K)	SST (°C)	Plot symbol
RF05	12 Jun 1992	40°46′N, 23°92′W	1719	740	340°/8.2	315.9	10.6		16.8	○
Flight 1		39°28′N, 24°05′W	2133	250	−0.1/0.9	−0.2	−1.8	3.1		
A209	13 Jun 1992	38°72′N, 23°13′W	0032	755	005°/10.3	313.7	10.0		17.2	□
Flight 2		37°52′N, 23°57′W	0426	240	−0.6/1.8	3.2	−1.2	4.5		
RF06	13 Jun 1992	37°43′N, 23°50′W	0451	770	010°/10.3	315.0	10.3		18.3	◊
Flight 3		35°78′N, 23°56′W	1013	280	−0.6/1.5	2.8	−0.9	3.8		
RF07	13 Jun 1992	34°81′N, 25°69′W	1627	1070	025°/8.9	317.7	10.3		20.1	+
Flight 4		32°89′N, 26°36′W	2109	610	−0.7/0.9	−2.7	−3.0	3.2		
A210	14 Jun 1992	28°79′N, 27°93′W	1111	1600	045°/3.5	317.3	9.5		21.1	△
Flight 5		28°71′N, 28°34′W	1302	500	−0.7/0.5	−6.6	−4.5	4.5		

etrate into the inversion. The cloud layer was multilayered with a cumulus layer developing below, which was acting to gradually form a stratocumulus layer and also penetrated into the stratocumulus layer above, with some even reaching the inversion. Several cumulus cloud were detected at 470 m with average liquid water contents of approximately 0.1 g kg^{-1}, suggesting that their cloud base was located at about 400 m. Between the cumulus and stratocumulus layers the turbulence activity was rather weak. Drizzle was seen to fall from the cumuli.

5) FLIGHT 5

On the last flight, which was undertaken during daytime, cumulus clouds dominated the turbulence, penetrating into the thin and broken stratocumulus clouds above (de Roode and Duynkerke 1996). Drizzle fell from the cumuli but did not reach the surface.

3. Data processing

a. Instrumentation

The instrumentation used aboard the MRF is described in Duynkerke et al. (1995) and de Roode and Duynkerke (1996). On flights of the Electra, described by Wang and Lenschow (1995), an instrumental fault in the pyrgeometer yielded unrealistic longwave radiative values. Therefore we did not use these data. Temperature measurements were made with a Rosemount resistance wire and were checked for unrealistic spikes due to wetting. On the flights we analyzed, we did not find any evidence of the above. In the unfiltered spectra of temperature and horizontal and vertical velocities we did not find any indication of instrumental malfunctioning. Humidity fluctuations were measured with a Lyman-alpha fast response hygrometer. Intermittent wetting of the Lyman-alpha affected some of the humidity measurements in cloud. Forward Scattering Spectrometer Probe (FSSP) measurements were used to determine the horizontally averaged liquid water content. On average, these data were in good agreement with average liquid water contents derived from the J–W instrument, except for the FSSP giving slightly higher values. The King Probe data were used to determine the liquid water flux. The use of two different aircraft makes it possible to compare results from Flights 2 and 3. The time lag between these two flights was very small and they flew in nearly the same air mass. As will be shown in section 4, it was found that the fluxes and variances during these two flights were very similar.

b. Flight strategy and data treatment

As part of the experimental strategy three different methods of making measurements were used: a nearly vertical profile, a horizontal run, and a porpoising run. To determine the mean state we used data from the horizontal runs instead of the profiles. For the stratocumulus cases cloud-top jumps were derived from the porpoising runs, whereas for the broken cloud field during Flight 5 this was done by subtracting the mean from horizontal legs just below and above cloud top because the jumps measured from the porpoise runs are very dependent whether the aircraft penetrates the inversion from clear or cloudy air.

To calculate vertical fluxes we used filtered data. The filter used is described by Nicholls (1989). We calculated a 31-sec running mean and subtracted it from the raw data, whereupon we applied the eddy correlation technique. This enabled us to filter out variations larger than about 3 km, thus neglecting the wavenumber contribution to the flux below the spectral peak. From the Eulerian integral length scale (Lenschow et al. 1994) we estimated the error in the second-order moments to be about 20% for the stratocumulus cases. Due to sampling and technical limitations in cloud the accuracy in the water vapor fluxes is less good and is estimated at

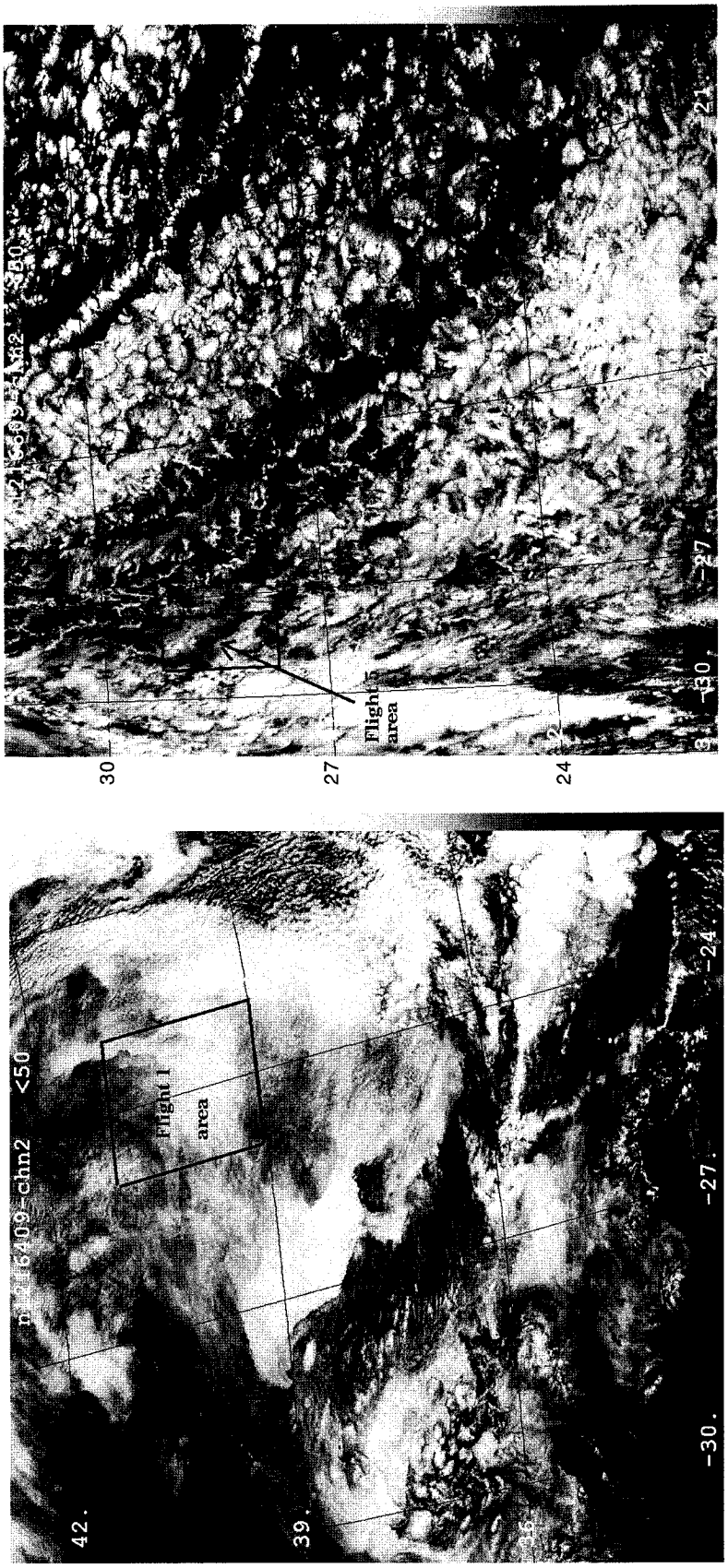

FIG. 1. (a) The NOAA AVHRR channel 2 satellite picture for 0945 UTC 12 June 1992 and (b) 0900 UTC 14 June 1992. Indicated are the longitude, latitude, and the flight area. The time interval between the cloud picture and the first horizontal flight is about 8 h for Flight 1 and 2 h for Flight 5.

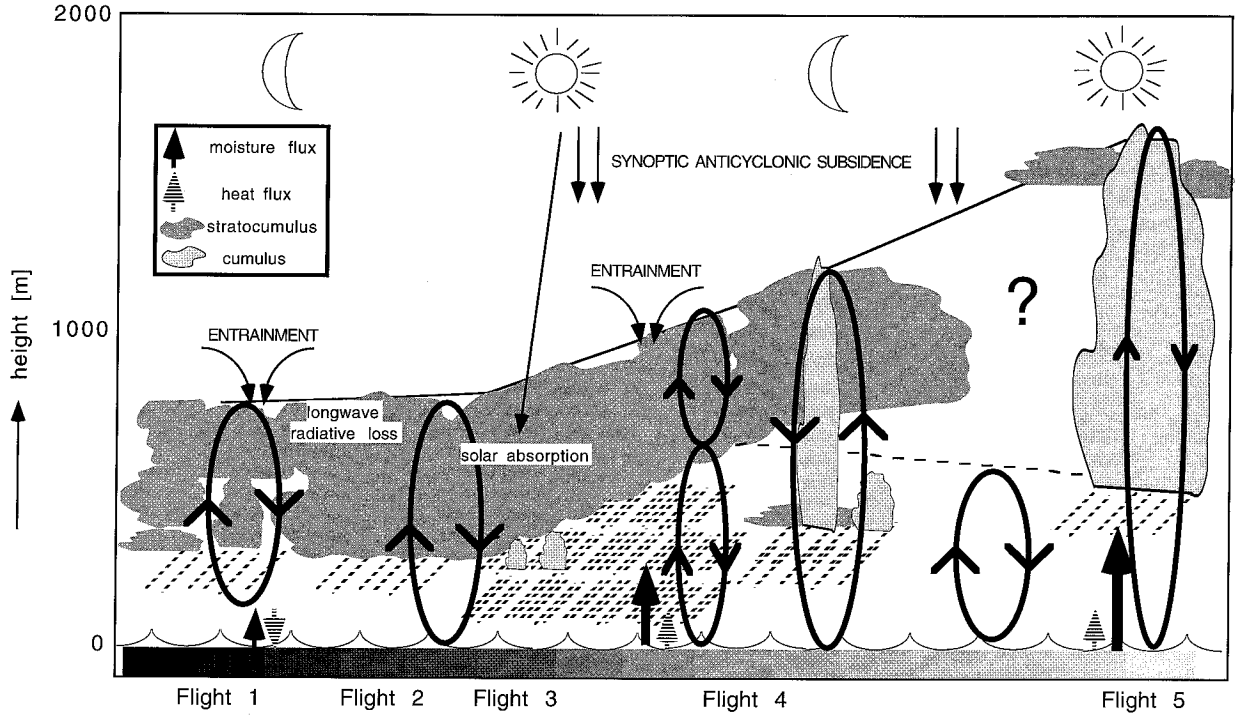

FIG. 2. A schematic of the cloud evolution as observed during the First Lagrangian of ASTEX between 1719 UTC 12 June 1992 and 1302 UTC 14 June 1992. The flights are indicated below the horizontal border. The horizontal distance between Flights 1 and 5 is approximately 1300 km. The grayscale in the lowest horizontal bar represents changing sea surface temperature, with increasing values from left to right. Fluxes of moisture and heat and cloud type are indicated according to the legend. The magnitude of the arrow is proportional to the flux. Day–night changes are schematically represented by the sun or moon symbol.

about 50%. For the fluxes during Flight 5, the error varied between 10% and 40%. The results shown of this flight represent horizontally averaged values over the entire flight leg and thus include both the cloudy and clear parts. The role of large scales in their contribution to the total vertical flux is not completely clear. For example, without filtering spectra of temperature and horizontal wind velocities do not show a spectral peak. In dry convective boundary layers similar observations were found from aircraft observations (Young 1987). Here the maximum amplitude of the vertical velocity spectra occured at a wavelength of 1.5 times the boundary layer height, but the maximum amplitude of the temperature spectra increased and shifted to longer wavelengths with height. However, in the study described in this paper we have neglected these large-scale effects, because the accuracy of the large-scale contributions to the flux is relatively uncertain due to the typical aircraft sampling length of about 60 km, which means that the large scales are not sufficiently sampled.

4. Mean state

As the boundary layer can be horizontally inhomogenous, we calculated the horizontal averages of the virtual potential temperature (θ_v), water vapor (q_v), liquid water (q_l), and the equivalent potential temperature (θ_e) from the horizontal runs. The vertical mean profiles of these horizontal averages are shown in Figs. 3a–d. Due to a relatively cold sea surface the surface layer was observed to be stable during Flight 1. As the air mass gradually moved southward over an increasing SST the surface layer became unstable, starting with Flight 2. The mean virtual potential temperature in the boundary layer decreased from Flight 1 to Flight 2 but during the last four flights it increased by about 5 K. It is remarkable that the virtual potential temperature in the free troposphere is nearly constant with time. When we neglect the contribution of horizontal advection (BAS) and solar absorption above the cloud layer, it suggests that warming due to subsidence is in equilibrium with the longwave radiative cooling.

The water vapor variations in the boundary layer are very small with time, suggesting that the input of moisture by a turbulent flux from the surface is in balance with drying by precipitation reaching the surface and entrainment of dry air from the free atmosphere. The mean liquid water content increased from about 0.2 to 0.6 g kg^{-1} between Flights 1 and 2. Since the BL temperature decreased between these two flights, the saturated mixing ratio must have decreased too, which may explain the observed increase in the liquid water content. Also, during Flight 1 the cloud deck was very

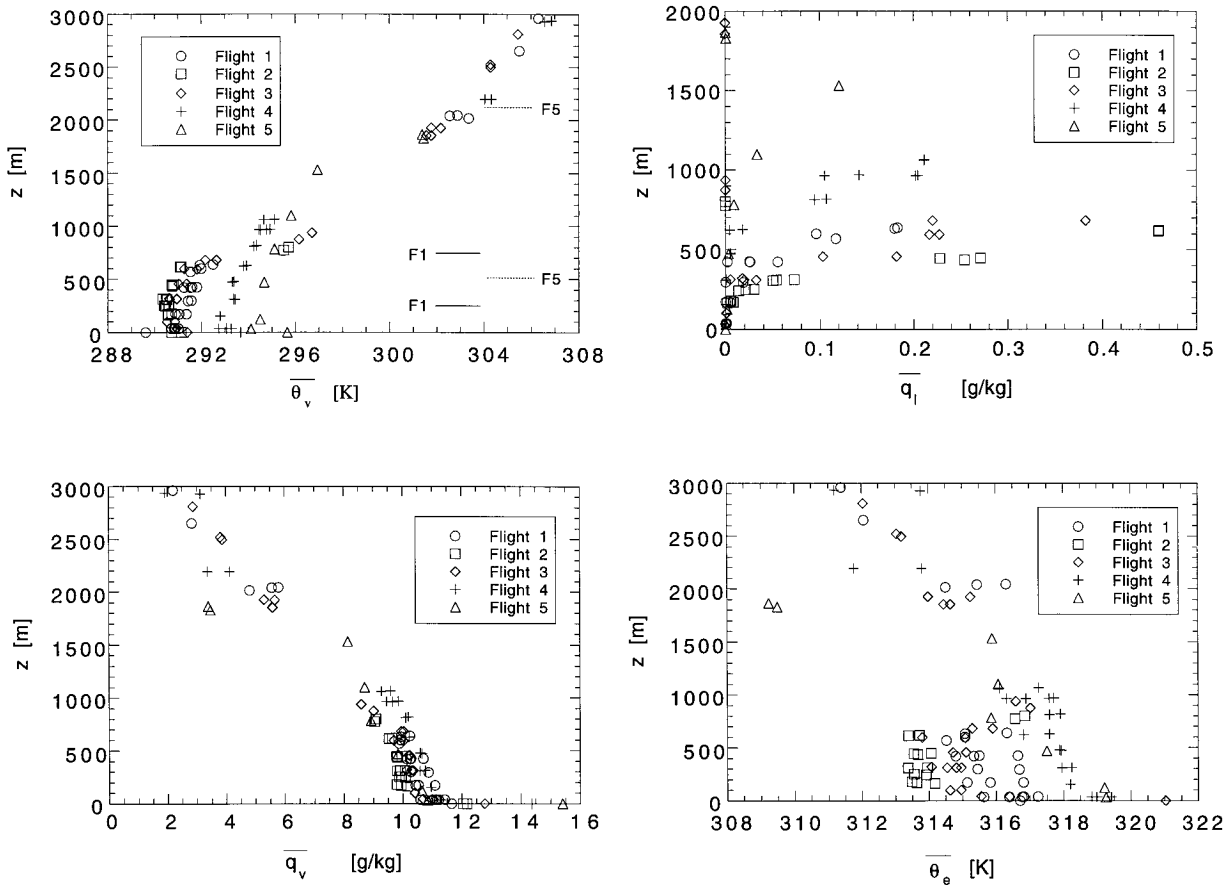

FIG. 3. Vertical mean profiles derived from the horizontal aircraft legs of (a) the virtual potential temperature, where cloud top and base are indicated by solid lines for Flight 1 ('F1') and dotted lines for Flight 5 ('F5'); (b) water vapor content; (c) the liquid water content; and (d) the equivalent potential temperature. Symbols are according to the legend.

inhomogeneous with clear patches within the cloud layer.

The cloud fraction shown in Figs. 4a–c was calculated from the FSSP measurements by counting the fraction of measurements where the liquid water content exceeded 0.001 g kg^{-1}. We estimated the cloud base and top from the porpoise runs and the vertical profiles (see Table 1). During Flight 1 only in the upper part of the cloud was the cloud fraction found to be about 1; in the lower part the cloud structure was found to be broken. Below cloud base some showers and foggy patches were found, which is obvious from the nonzero cloud fractions. During Flights 2 and 3 the cloud is more solid, with a maximum cloud fraction of 1 between 450 and 700 m. In the middle of the cloud layer for Flight 4 it is difficult to distinguish the cumulus from the stratocumulus, but the cloud fraction at the lower levels is probably due to cumuli. For Flight 5, the cloud fraction between 500 and 1100 m represents the cumulus cloud fraction, whereas at 1530 m the cloud fraction is the sum of cumulus and broken stratocumulus (de Roode and Duynkerke 1996).

5. Turbulence structure

a. Scaling

Since the structure of the boundary layer turbulence varies considerably with time, we will not attempt to scale the turbulent fluxes measured during the five flights using similarity arguments because the boundary conditions differed too much for each flight. For example, it is difficult to account for the effects of solar radiation and drizzle. However, because the First Lagrangian is an ideal case for model studies, we calculated some typical scaling quantities from the observed fluxes. The increase in u_*, T_{v*}, and q_{T*} from Flight 1 to Flight 4, as shown in Table 2, indicates an enhanced surface input of moisture, heat, and momentum into the boundary layer. According to the values of the Monin–Obukhov length scale, this is due to the transition from a stable to a more unstable surface stratification. This mechanism partially explains the increasing convective velocity w_*. Furthermore, during Flight 4 large positive virtual potential temperature fluxes in the cloud layer made a significant contribution to w_* as well.

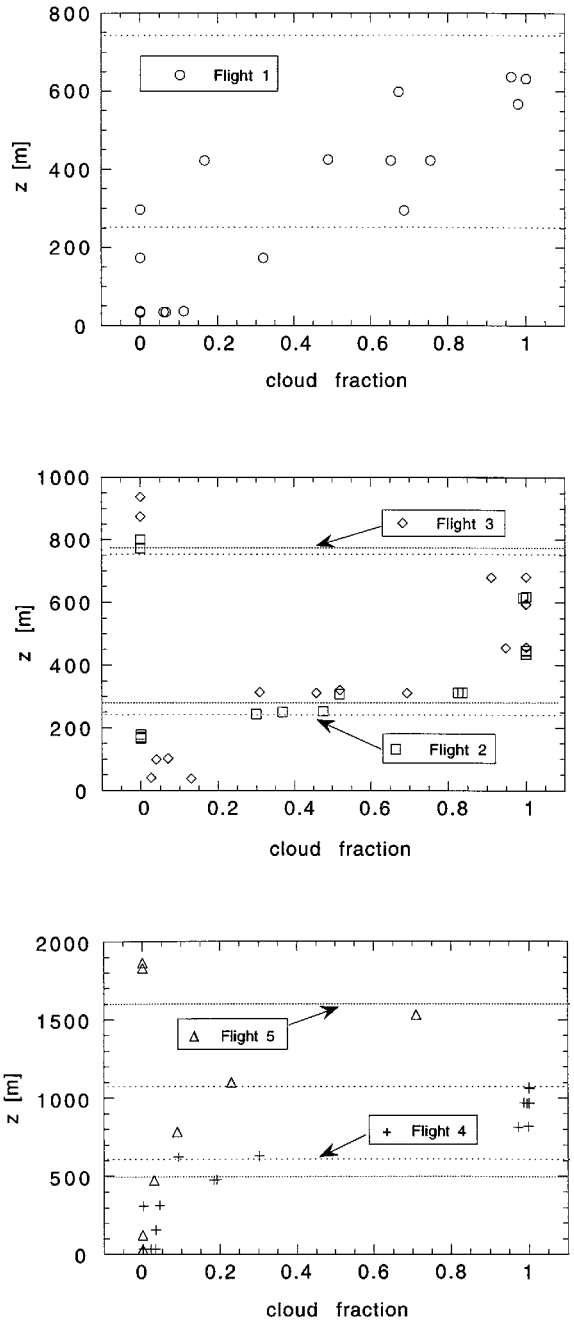

FIG. 4. The cloud fraction for (a) Flight 1, (b) Flights 2 and 3, and (c) Flights 4 and 5. Horizontal lines represent the cloud base (lower) and cloud top (upper). Plot symbol and line style are indicated by arrows and legend.

The results of the turbulence during the five flights are grouped and shown in three different graphs for clarity. The first graph presents the results of Flight 1 since it was the only case with a stable surface stratification. In the second plot the results of Flight 2 and 3 are shown together since the turbulence characteristics are very similar. The third graph shows the last two flights. Although these flights do have quite different characteristics, we combined these in one graph simply to reduce the number of plots.

b. Virtual potential temperature flux

The virtual potential temperature flux $\overline{w'\theta_v'}$ can to a good approximation be expressed as

$$\overline{w'\theta_v'} = \overline{w'\theta'} + \bar{\theta}(0.61\overline{w'q_v'} - \overline{w'q_l'}), \qquad (5.1)$$

where $\overline{w'q_v'}$ and $\overline{w'q_l'}$ are the water vapor and liquid water flux. During the time of the First Lagrangian the buoyancy flux at the surface increased from a slightly negative value of -0.002 K m s^{-1} to a positive flux of about 0.015 K m s^{-1} during Flight 2 (see Figs. 5a–c). This is in accordance with the aerodynamic bulk formulas used by BAS. All flights in stratocumulus show a maximum buoyancy flux near the cloud top, which can be explained by negatively buoyant downdrafts formed by longwave radiative loss. However, during Flight 4 the fluxes near the cloud-top maximum were about a factor of 3 or 4 higher relative to the previous flights. According to the maximum buoyancy flux near cloud top during Flight 4, it is unlikely that the cumulus clouds made a significant contribution to the buoyancy flux. For these kind of clouds, the maximum buoyancy flux is found just above the cloud base, whereas near the cloud top the buoyancy flux is very small or even negative due to overshooting of cloudy air parcels (Cuijpers et al. 1996; Smith and Jonas 1995).

We can express the buoyancy flux in a cloud as (Nicholls 1984)

$$\overline{w'\theta_v'} = \beta\overline{w'\theta_e'} - \theta\overline{w'q_t'}, \qquad (5.2)$$

where β is a function of the temperature and is typically about 0.6 and the turbulent flux of total water is $\overline{w'q_t'} = \overline{w'q_v'} + \overline{w'q_l'}$. Here we neglected the effects of gravitational settling of droplets at the top of the cloud. Using Eq. (5.2) and Lilly's (1968) relationship for the entrainment velocity w_e,

$$w_e = -\frac{\overline{w'x'}_H}{\Delta\bar{x}}, \qquad (5.3)$$

where $\overline{w'x_H'}$ is the flux of a conserved variable at the top of the BL and Δ represents the mean jump across the inversion; then the virtual potential temperature flux at the top of the cloud can be written as

$$(\overline{w'\theta_v'})_H = w_e[-\beta\Delta\bar{\theta}_e + \theta\Delta\bar{q}_t]. \qquad (5.4)$$

This result is valid for adiabatic processes only; thus drizzle and radiative processes are not included. Using the jumps given in Table 1 we evaluated the term in square brackets in Eq. (5.4) and found values of -0.4, -1.6, -1.9, and 0.8 for Flights 1–4, respectively. This means that entrainment ($w_e > 0$) will cause a positive buoyancy flux at the top of the cloud for Flight 4. In other words, when air from above the inversion is entrained, the evaporation of cloud droplets can compensate (and even can cause a net cooling) for the mixing

TABLE 2. Characteristic turbulent scales w_*, u_*, T_{v*}, q_{T*}, L, and Ri_{w*} (Nicholls 1989; Nicholls and Turton 1986) during the First Lagrangian. Here H represents the boundary layer depth; w the vertical velocity; T_v the virtual temperature; g the acceleration due to gravity; z the height above sea level; u and v the eastward and northward velocity, respectively; q_v the water vapor; and q_l the liquid water content. The subscript $_s$ denotes the surface value, which we extrapolated from measurements of the lowest legs. The value used for the von Kármán constant is $k = 0.4$.

		Flight 1	Flight 2	Flight 3	Flight 4	Flight 5
$w_* \equiv \left\{2.5(g/\bar{\theta}) \int_0^H \overline{w'\theta_v'}\, dz'\right\}^{1/3}$	(m s^{-1})	0.63	0.66	0.66	0.9	0.64
$u_* = \left(\overline{u'w_s'}^2 + \overline{v'w_s'}^2\right)^{1/4}$	(m s^{-1})	0.19	0.26	0.28	0.28	0.14
$T_{v*} = \dfrac{w_*^2\bar{\theta}}{gH}$	(K)	0.016	0.017	0.017	0.023	0.010
$q_{t*} = \dfrac{\left(\overline{w'q_v'} + \overline{w'q_l'}\right)_s}{w_*}$	(g kg^{-1})	0.008	0.011	0.027	0.022	0.030
$L = \dfrac{-u_*^3}{k\cdot\dfrac{g}{\bar{\theta}_v}\cdot\left(\overline{w'\theta_v'}\right)_s}$	(m)	500	−170	−100	−120	−30
$\mathrm{Ri}_{w*} = \dfrac{gH}{\bar{\theta}_v}\dfrac{\Delta\bar{\theta}_v}{w_*^2}$		195	261	220	142	592

of warm free atmospheric air into the cloudy BL. This mechanism possibly explains the increased virtual potential temperature fluxes in the cloud layer as observed during Flight 4 compared with the previous flights. When the term within brackets in (5.4) is negative, as for Flights 1–3, the role of entrainment is to reduce the effect of cooling by the longwave radiative loss at the top of the cloud and hence a reduction of the maximum buoyancy flux in the cloud.

c. Water flux

Under horizontally homogeneous conditions the equation for the total water content as a function of time can be written as

$$\frac{\partial\overline{q_t}}{\partial t} = -\frac{\partial\overline{w'q_t'}}{\partial z} - \frac{\partial\widetilde{w'q_l'}}{\partial z}, \tag{5.5}$$

where $\widetilde{w'q'}_l$ is the drizzle flux calculated according to the measurements of the droplet size concentrations. The droplet terminal velocity w_T as a function of droplet radius (r) is given by (Rogers 1979):

$$\begin{cases} w_T(r) = 1.19 \times 10^8 r^2 & \text{for } r < 40 \times 10^{-6} \text{ m} \\ w_T(r) = 8 \times 10^3 r & \text{for } r \geq 40 \times 10^{-6} \text{ m.} \end{cases} \tag{5.6}$$

The droplet spectrum was measured by an FSSP (MRF and Electra), a Particle Measurement Systems (PMS) 2DC probe (MRF), and a PMS 260X (Electra) probe. Assuming that the drizzle flux at the top of the BL is zero and integrating Eq. (5.5) we can, for a well-mixed layer, express the average total water content as a function of time:

$$H\frac{\partial\overline{q_t}}{\partial t} = -(\overline{w'q_t'})_H + (\overline{w'q_t'})_s + (\widetilde{w'q_l'})_s, \tag{5.7}$$

where H is the boundary layer height and the subscript s denotes the surface value. From the mean profiles in Fig. 3b it was found that the average total water content did not vary much with time, suggesting that the three terms on the rhs of Eq. (5.7) balance each other. Since drizzle and entrainment are sink terms, the surface flux must balance these two terms. From the flux measurements it is difficult to calculate the moisture budget accurately since the precipitation rate can vary much with time and space.

The total water fluxes near the cloud top increased from Flight 2 to Flight 4 (Fig. 6), indicating that gradually more dry air is mixed into the BL by entrainment, which possibly reflects the fact that during these flights the total water jump across the inversion increased. In the cloud layer the drizzle flux is of the same order of magnitude as the total water flux. From the lowest legs during Flight 3 it is observed that drizzle effectively reached the surface, thereby removing water from the BL. On the other hand, the gradient in the vertical drizzle profiles during Flights 2 and 4 suggest that there is a significant evaporation of drizzle in the subcloud layer; this will cool and moisten this layer by redistributing water from the upper cloud layer downward. During Flight 5 the opposite was found (not shown here); in this case there was an upward transport of moisture by

the cumuli from the subcloud layer to the cloud top (de Roode and Duynkerke 1996). During Flight 1 three measurements showed significantly higher drizzle rates. Since all these measurements were done during the last part of Flight 1, it probably took place in a local shower.

d. Velocity variance and TKE

The vertical velocity variances are shown in Figs. 7a–c. During Flight 1 the turbulence is rather weak in the subcloud layer since turbulent fluctuations are damped by the stable surface stratification. In the cloud layer there is a large scatter of results, possibly due to the complicated two-layer cloud structure.

The vertical velocity variances during Flight 5 are on average much weaker than during Flight 4 because in the last flight the turbulence was dominated mainly by broken cumulus clouds and in between these clouds the boundary layer was nearly laminar. However, for both cases two vertical velocity variance maxima were found in the subcloud and cloud layers, suggesting these two layers were decoupled. During Flight 4 the meteorological observer aboard the aircraft remarked that cumulus clouds seemed to be forming a cloud layer beneath the stratocumulus deck with a nearly laminar layer in between. Since Flight 4 started just before sunset, a likely explanation for this decoupling is the absorption of solar radiation in the cloud layer (Rogers et al. 1995). Another possible mechanism that supports decoupling is evaporation of drizzle and subsequent cooling in the subcloud layer (Nicholls 1984). In the upper part of the cloud layer during Flight 4 the vertical velocity variance was larger than during the other flights, which is in line with the increased buoyancy fluxes and the prediction that entrainment would generate TKE for this case.

A similarity curve for the vertical velocity variances derived from measurements in clear free convective boundary layer was proposed by Lenschow et al. (1980):

$$\overline{w'^2} = 1.8\left(\frac{z}{H}\right)^{2/3}\left(1 - 0.8\frac{z}{H}\right)^2 w_*^2. \qquad (5.8)$$

During Flights 2 and 3 the vertical velocity variance profiles were very similar to this curve (5.8). For both flights the buoyancy flux near the surface is of the same order of magnitude as at the cloud top. Thus, the convection driven from the surface is nearly as important as the convection driven from the cloud top. For Flight 1 we scaled the curve upside down for the boundary layer assuming that the turbulence is driven mainly by longwave radiative loss from the cloud top (Hignett 1991; Nicholls and Leighton 1986). In spite of the inhomogeneity of the cloud layer the average order of magnitude of the vertical velocity from observations is in good agreement with the fit upside down. Since during Flight 4 the boundary layer was decoupled, we calculated w_* separately for the subcloud and cloud layer (Hignett 1991), using the integral relationship as in Table 2 and the heights of these two layers. As in Flight 1, the curve fit was plotted upside down in the cloud layer for Flight 4. The similarity relationship (5.8) seems to predict the observed vertical velocity variance in the subcloud layer very well. The agreement in the cloud layer between the fit and observations is not as good as in the subcloud layer. For example, the maximum vertical velocity variances are underestimated, which was

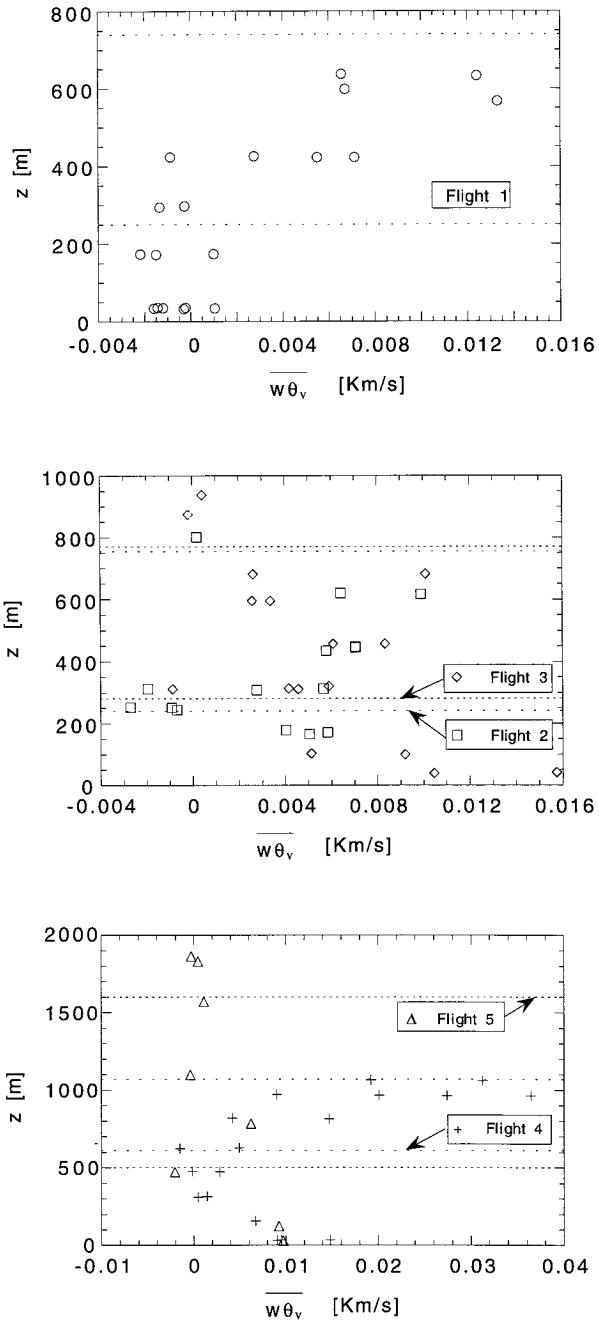

FIG. 5. The virtual potential temperature flux for (a) Flight 1, (b) Flights 2 and 3, and (c) Flights 4 and 5. Symbols and line styles as in Fig. 4.

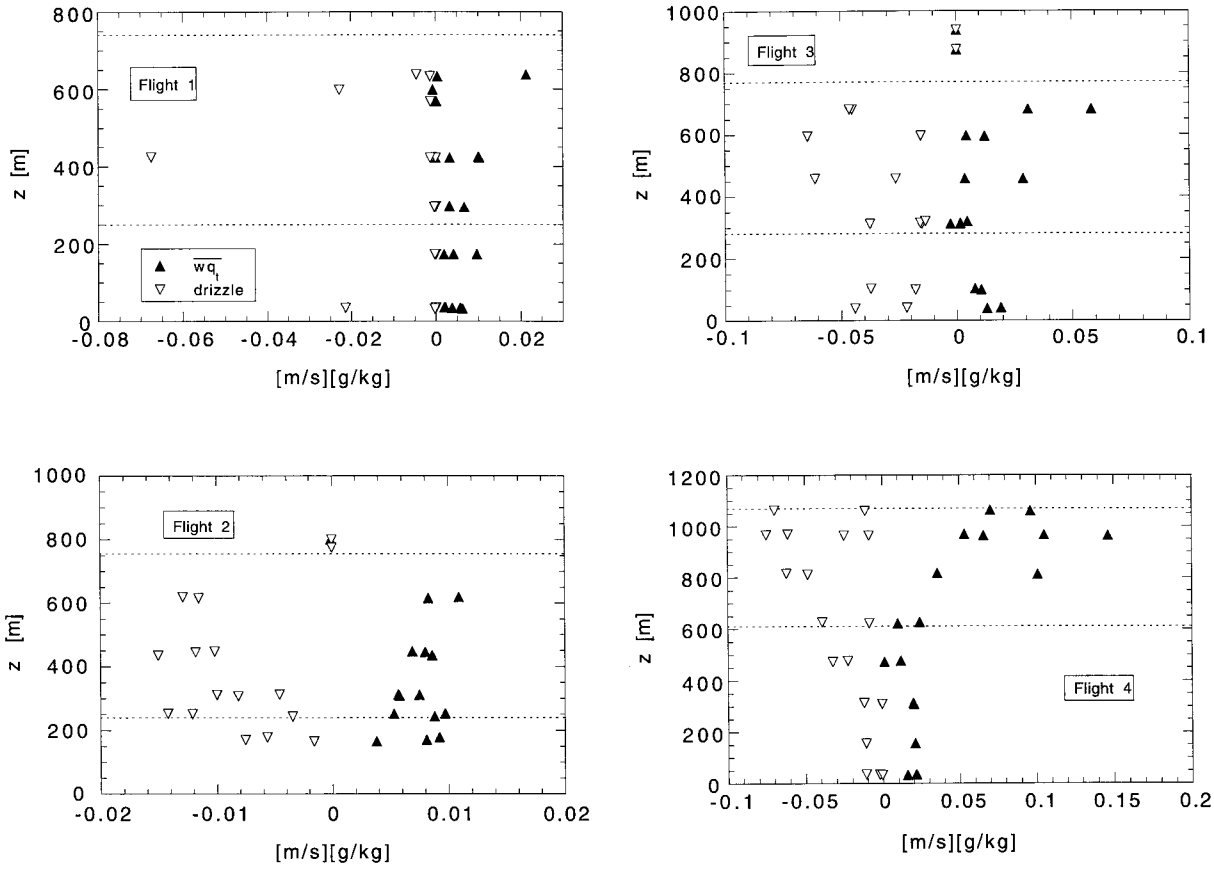

FIG. 6. The total water and drizzle flux for (a) Flight 1, (b) Flight 2, (c) Flight 3, and (d) Flight 4. Plot symbols as indicated in the legend.

also observed by Nicholls and Leighton (1986). These authors suggested that this possibly reflects that because of the small density jump across the inversion the interface can be more deformed in response to local vertical motions than a solid or liquid interface, thereby less damping of the vertical motions. Since the location of the vertical velocity maximum from the fit is in good agreement with the observed maximum, this suggests that the turbulence in the cloud layer is driven from the top.

Hignett (1991) analyzed measurements from nighttime and daytime stratocumulus and made a comparison with the similarity relationship (5.8). For the nocturnal cases the vertical velocity variances for the entire depth of the BL were used, while for the daytime cases only data of the cloudy mixed layer were selected because the cloud layer was observed to be decoupled. Overall, with the curve fit plotted upside down there was reasonable agreement with the observations. Nevertheless, these results contrast with the observations during Flights 2 and 3 because the vertical velocity variance maximum for these two cases was found in the lower half of the BL. Therefore, it is probably important where the maximum buoyancy flux is located. If it is longwave radiative cooling that predominantly drives the turbulence, it may be expected that the vertical velocity variance peak will be located in the upper half of the BL. On the other hand, if entrainment of warm air can, for a large part, compensate the longwave radiative loss and if the surface flux is relatively large (Duynkerke et al. 1995), this kind of cloud-topped boundary layer might be more similar to a dry convective BL.

The turbulence kinetic energy (Figs. 8a–c) does not show much variation with height for the first three flights. Since the vertical velocity variance in the subcloud layer was very weak during Flight 1, this implies that in this case the horizontal velocity variances in the subcloud layer are of the same order of magnitude as the vertical velocities in the cloud layer. Since the surface layer is stably stratified, the TKE in the subcloud layer must have been generated by a considerable wind shear. During Flights 4 and 5 the TKE in the boundary layer is not well mixed. Here there is a weak minimum near the cloud base, and there are maxima near the surface and the cloud top, reflecting the two-layered structure of the BL caused by decoupling.

e. Skewness

The skewness is defined as $S_w = \overline{w'^3}/(\overline{w'^2})^{3/2}$ and is a measure of the asymmetry in the vertical velocity fluc-

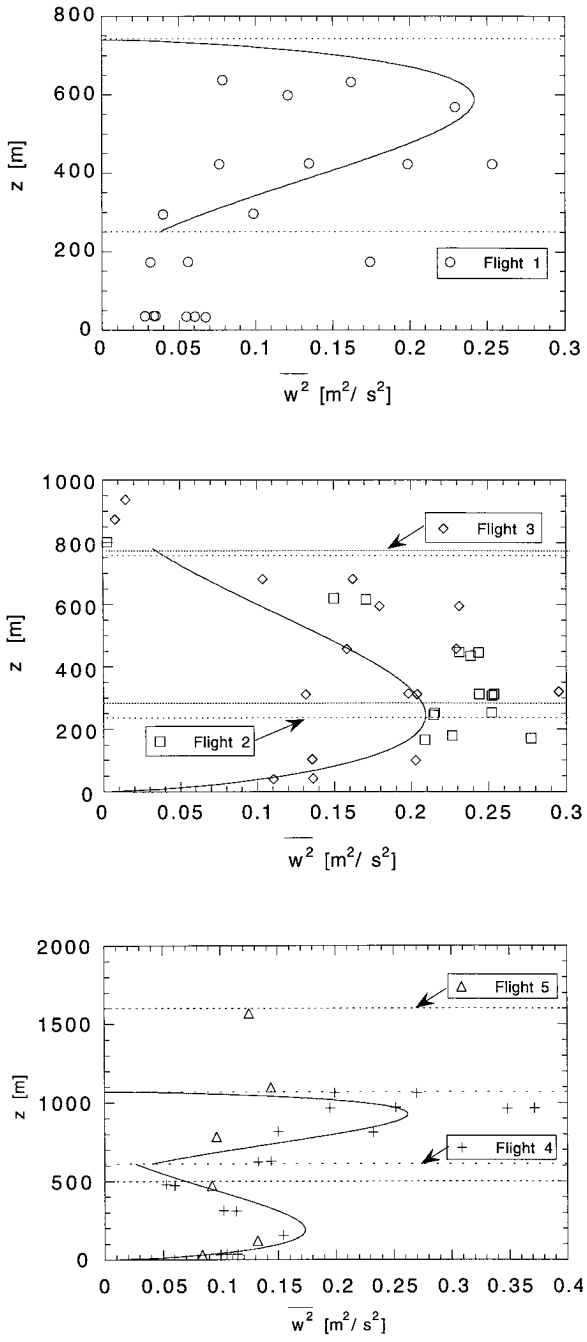

FIG. 7. The vertical velocity variances as a function of height for (a) Flight 1, (b) Flights 2 and 3, and (c) Flights 4 and 5. The curve in (a) and (b) is from Lenschow et al. (1980) representing $\overline{w'^2} = 1.8(z/H)^{2/3}(1 - 0.8z/H)^2 w_*^2$. The curve is scaled upside down for Flight 1. Symbols and line styles as in Fig. 4.

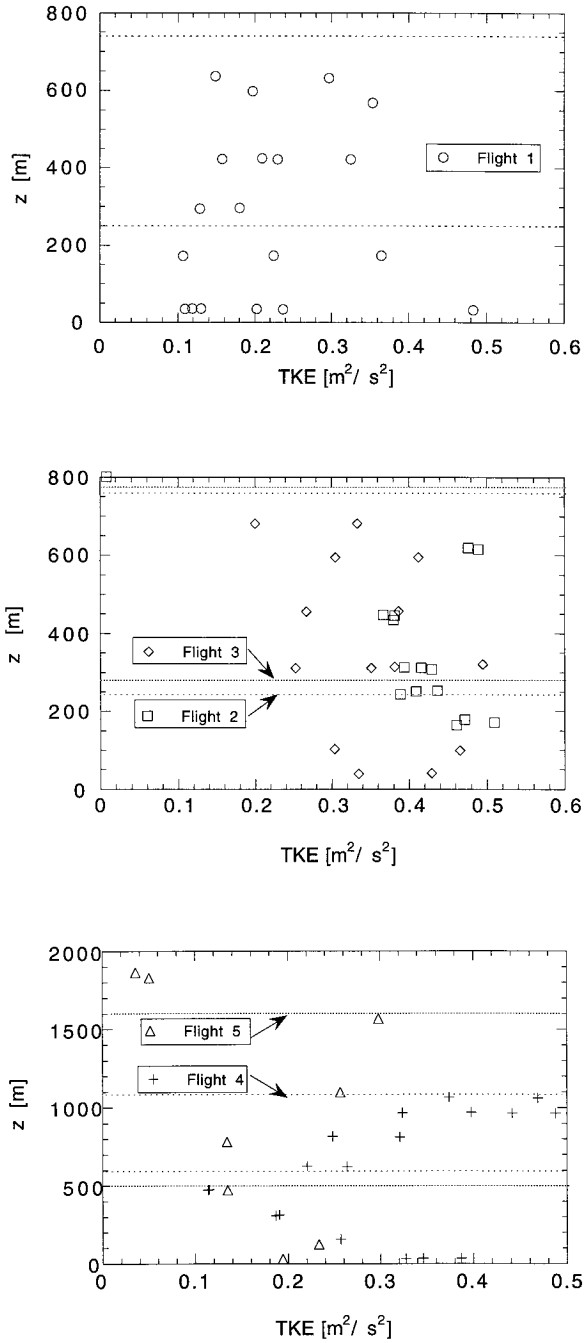

FIG. 8. The turbulent kinetic energy as a function of height for (a) Flight 1, (b) Flights 2 and 3, and (c) Flights 4 and 5. Symbols and line styles as in Fig. 4.

tuations. For example, if S_w is positive, it physically means that updrafts are more intense than downdrafts. On the other hand, Nicholls and Leighton (1986) observed that S_w became increasingly more negative with distance beneath cloud top up to a depth of a few hundred meters, suggesting that convection in the upper part of the cloud layer was predominantly driven by downdrafts as a result of cloud-top radiative cooling. The same results are found for Flight 1 (see Fig. 9a) for which the turbulence is, in particular, driven by longwave radiative loss because of the stable surface stratification. The gradual transition to warmer sea surface temperatures is obvious from the skewness found from

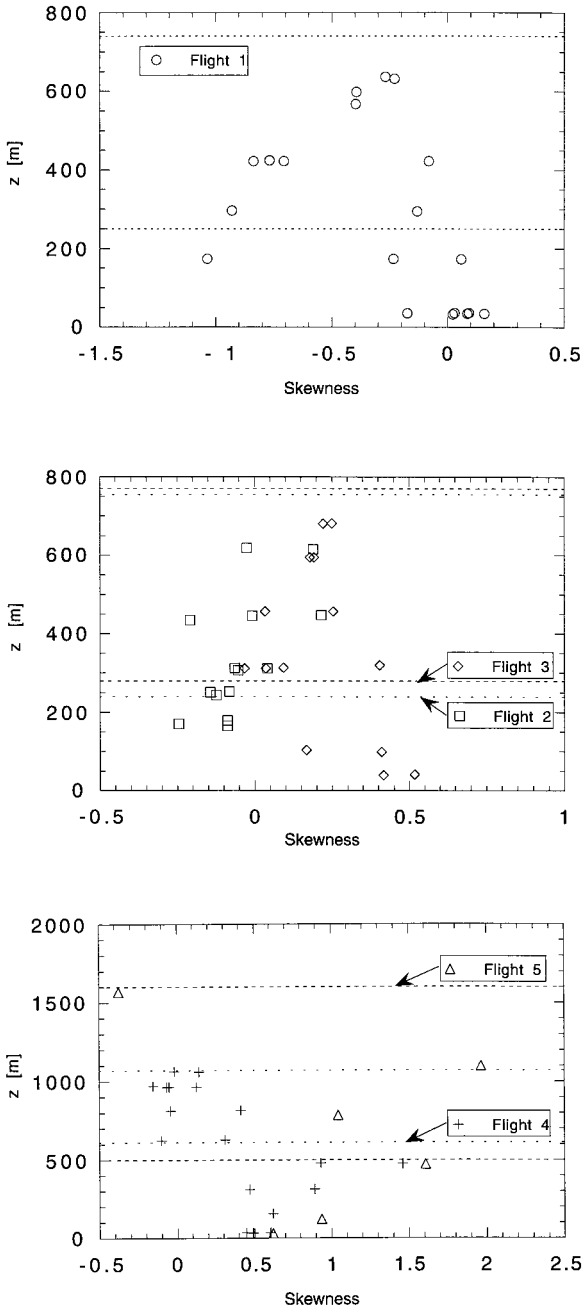

FIG. 9. The vertical velocity skewness S_w as a function of height for (a) Flight 1, (b) Flights 2 and 3, and (c) Flights 4 and 5. Symbols and line styles as in Fig. 4.

Flights 3–5 (Figs. 9b and 9c), showing that updrafts driven from the unstable surface dominate the convection in the subcloud layer. In the cloud layer of Flights 2 and 3 the skewness suggests that convection driven by the release of latent heat in the cloud is as strong as turbulence driven from the top by entrainment warming and subsequent radiative cooling. During Flight 5 the high value of the skewness reflects that in a cumulus cloud layer the updrafts can become very strong as a result of the release of latent heat in the cloud, which gives rise to compensating subsidence in the dry environment. The large skewness found at about 500 m on Flight 4 is probably due to cumulus activity that has its cloud base at approximately 400 m, while for Flight 5 the local maximum near cloud base is caused by a strong updraft in a local shower below the cumulus. Because of the small skewness in the cloud layer during Flight 4 it seems that cumulus clouds are not as dominant for the convection as observed during Flight 5 but are about equally important as convection driven from the top.

6. Cloud-top structure: Stability and entrainment

a. Cloud-top stability

The stability of the interfacial layer between a cloud deck and the overlying cloud-free air is of great importance for predicting the time evolution of the stratocumulus-topped boundary layers. Lilly (1968) pointed out that the evaporative cooling of unsaturated air entrained into the cloud can, under some conditions, cause this air to descend unstably as a convective downdraft. The negatively buoyant mixture enhances TKE at cloud top, which may cause even more overlying free tropospheric air to be entrained, thus enhancing this process. This feedback mechanism can possibly lead to the rapid dissipation of the cloud and is referred to as cloud-top entrainment instability. The exact form of the CTEI criterion has not yet been established. On the basis of the assumption that a parcel after mixing remains just saturated, Randall (1980) and Deardorff (1980) suggested that the criterion for instability should be

$$\Delta\overline{\theta_e} < K\,(L/c_p)\,\Delta\overline{q_T}, \tag{6.1}$$

where the constant K has a value of about 0.23 (the dotted line in Fig. 11) and L is the latent heat of condensation. The criterion (6.1) is actually the same equation as the term within brackets in Eq. (5.4), which was positive for Flight 4 and hence should be unstable.

MacVean and Mason (1990, hereafter referred to as MM) also studied the cloud-top entrainment instability mechanism by investigating the possible conditions for free mixing at an interface with different thermodynamical properties. They suggested that K should have a value of about 0.7 (the long-dashed line in Fig. 11). Duynkerke (1993, hereafter referred to as DK) introduced a stability parameter Δ_a, based on the time integral of the buoyancy excess during a parcel's lifetime from its unmixed state to a state in which its properties are overwhelmed by the properties of the surrounding air (solid line in Fig. 11).

To calculate the inversion jumps we used the data measured during the porpoising runs. An example of these time series, shown in Fig. 10, clearly illustrates the relatively rapid changes of potential temperature,

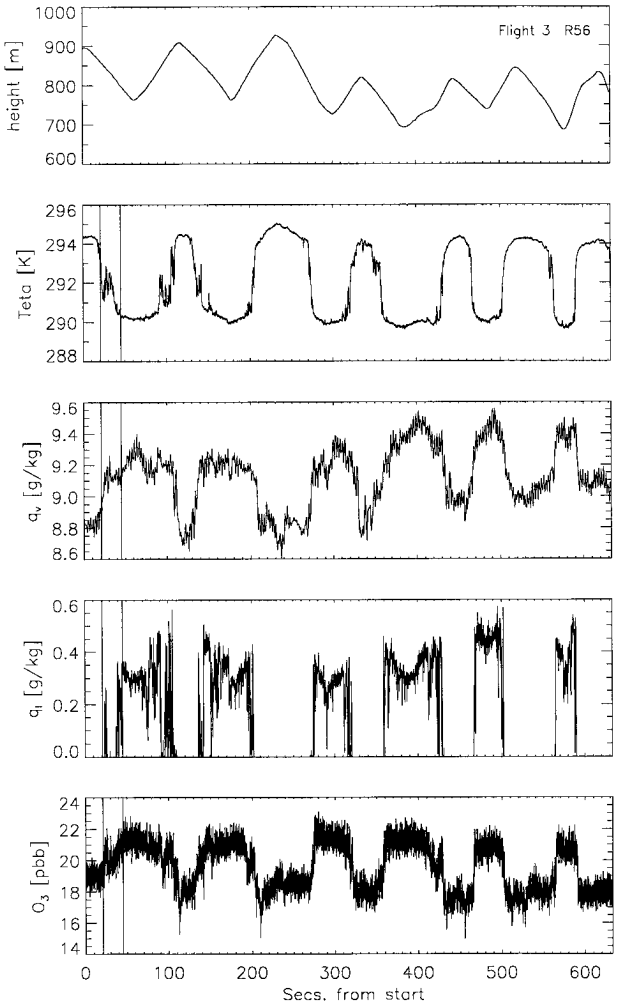

FIG. 10. Time series of the aircraft height, potential temperature, water vapor content, liquid water content, and ozone concentration measured during the porpoise run R56 on Flight 3.

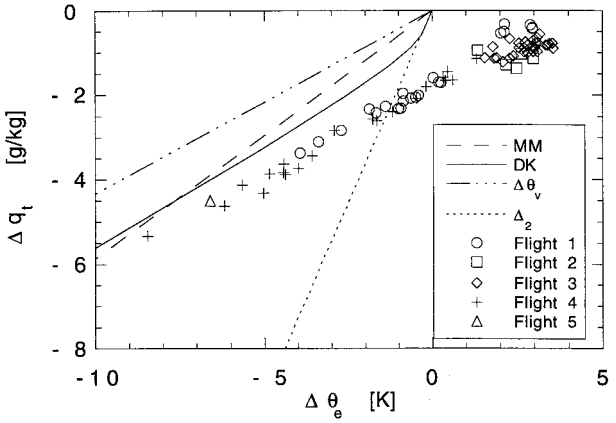

FIG. 11. Observations of Δq_t and $\Delta\theta_e$ made in solid stratocumulus as observed during Flights 1–4 and broken stratocumulus and cumulus clouds (Flight 5, one point). The lines represent the different stability criteria: dry adiabatic $\Delta\theta_v = 0$ (dash-dotted); wet adiabatic $\Delta_2 = 0$ [dotted; see Randall (1980) and Deardorff (1980)]; stability criterion of MacVean and Mason (1990) (long dashed); and $\Delta_a = 0$, stability criterion of Duynkerke (1993) solid line for $q_{12} = 0.5$ g kg^{-1}). For plot symbols see legend.

mixing ratio, liquid water, and ozone across the inversion. However, measurements between 21 and 45 sec, for example, show liquid water variations indicating the aircraft is flying in cloudy patches, while the potential temperature, the liquid water content, and ozone concentration show variations superposed on a approximate linear line connecting the BL with free atmosphere values. These variations are due to local variations in the cloud-top height but are also indications of the entrainment interface layer (Caughey et al. 1982; Nicholls and Turton 1986). In this layer several tens of meters deep a mixture between cloudy and the inversion air is present. Because this layer contains a mixture of air, we tried to detect this layer to omit these measurements for the calculation of the inversion jump. For each individual penetration the EIL was determined as the layer with very strong fluctuations located between two layers with relatively small vertical gradient and less variations. For ozone, temperature, and water vapor the inversion jump was determined as the difference between the average free atmosphere and BL value, while the maximum liquid water content found on each individual penetration was used in determining the total water jump.

The variation in the jumps during one flight is considerable (see Fig. 11). On Flight 3 two series of porpoising runs were made separated by an interval of about 140 minutes. The calculation of the average jumps for these two series separately did not show a significant change in the jumps (0.11 g kg^{-1} and 0.43 K for the total water content and equivalent potential temperature, respectively; see Table 3). Therefore, the variation in the jumps is merely caused by horizontal variations in the boundary layer or inhomogeneities in the free troposphere than by time variations. This is quite obvious from the total water jumps during Flights 1 and 4, which show differences of about 2 g kg^{-1} between two porpoising runs in perpendicular directions. The jump of Flight 5 is calculated from the horizontal legs just between and above the inversion and lies in the same range as Flight 4. A similar analysis was performed by Kuo and Schubert (1988). The data these authors were examining were collected from nine papers describing stratocumulus cases in the midlatitudes and subtropics and one case of trade cumulus clouds. From their diagram they found that the jumps were approximately arranged along the line $\Delta\theta_l = 9$ K [where $\theta_l = \theta - (L/c_p)\, q_l$, the liquid water potential temperature] and that 32 out of 48 of the stratocumulus cases were unstable following the criterion (6.1). During the First Lagrangian, only during Flights 2 and 3 are the measured inversion jumps all stable according to CTEI criterion (6.1), while during Flight 4 the majority of jumps are in the unstable regime, which is also the case for the single jump measured in the broken stratocumulus/cu-

TABLE 3. Observed jumps derived from the porpoising runs of the Electra aircraft. The ozone jumps used for the calculation of the entrainment rate are indicated with '(*)'.

Flight	Run	Number of penetrations	Orientation	ΔO_3 (ppb)	$\Delta\theta_v$ (K)	Δq_T (g kg^{-1})	$\Delta\theta_e$ (K)
1	R71	16	northeast–southwest	3.91 (*)	3.40	−2.26	−1.23
	R72	6	northwest–southeast	−0.99	2.44	−0.43	2.51
3	R25	8	east–west	−1.31	3.36	−0.95	2.29
	R26	4	north–south	−1.70	3.71	−0.97	2.73
	R55	3	south–north	−3.19 (*)	3.63	−0.83	2.78
	R56	12	west–east	−2.97 (*)	4.18	−0.87	3.10
4	R37	11	southwest–northeast	−0.39	3.13	−2.03	−0.52
	R38	10	northwest–southeast	4.61 (*)	3.32	−4.02	−5.03

mulus field during Flight 5. Because θ_e is linearly dependent on q_T, the jumps can be fitted along a straight line as well. However, the observed jumps seem to fit better along the line $\Delta\theta_l = 5$ K. Since during the First Lagrangian the jumps in the liquid water content across the stratocumulus cloud top are generally of order 0.5 g kg^{-1}, this difference is mainly due to a smaller potential temperature jump during the First Lagrangian than in the cases summarized by Kuo and Schubert (1988).

All of the measured cloud-top jumps suggest that the cloud should be stable according to the criteria of MM and DK, with Flights 1 and 4 having some jumps very close to these two curves. It is remarkable that from Flight 2 to 4 the cloud-top jumps approach these two curves; this is due to the jumps in the equivalent potential temperature and total water content becoming more negative. From Table 1 we found that during these flights the mean equivalent potential temperature and total water content in the boundary layer increased by 3 K and 0.3 g kg^{-1}. Therefore warming and, to a lesser extent, moistening of the boundary layer can explain the decreased equivalent potential temperature jump. In particular, during daytime the cloudy air was warmed by the absorption of solar radiation between Flights 3 and 4. In addition, the subcloud layer was continuously warmed by the warmer sea surface. Also, because of a negative gradient of the equivalent potential temperature and total water content above the BL, the effect of entrainment is not only to increase the BL height, but also to decrease the value of these variables on top of the higher inversion.

b. Entrainment

The entrainment rate is crucial for the boundary layer evolution since it is a measure of the mixing of relatively warm and dry air of free tropospheric origin into the cloudy boundary layer. Therefore, we calculated the entrainment velocity using the turbulent fluxes of ozone, total water, and the equivalent potential temperature. We selected measurements made solely in the cloud layer because this layer can be assumed to be well mixed and, thus, problems with decoupling or stable surface stratification can be avoided. A linear fit through all the in-cloud measured fluxes was made in order to extrapolate the flux at the top of the cloud. The entrainment rate was calculated from this extrapolation using Eq. (5.3) and the jumps according to Table 1 (total water and equivalent potential temperature) and Table 3 (ozone). This method was also applied by BAS, who used only ozone fluxes for the highest below inversion legs of the Electra. However, from the analysis of the porpoise runs we found that the ozone jumps were dependent on the flight direction (see Table 3), in particular during Flights 1 and 4. For these two cases we only used in-cloud fluxes of ozone that were measured both in the same flight direction and just before or after the porpoise runs. We rejected cases where the absolute values of the jumps across the inversion were smaller than 1 ppb for ozone and 1 g kg^{-1} for the total water content. Also, we did not use the ozone fluxes measured just before the porpoising legs R25/R26 of Flight 2 because these levels were approximately 200 m below the average cloud top, which makes an extrapolation for the cloud-top flux rather unreliable. For the total water flux we did not take drizzle into account and, therefore, this method will probably overestimate the entrainment velocity. The equivalent potential temperature flux was used for Flight 2 because it was made at night and therefore could be corrected for longwave radiative loss near the top of the cloud (Duynkerke et al. 1995):

$$w_e = \left\{ \frac{1}{\rho c_p}(F_{H_-} - F_{z_m}) - \overline{(w'\theta_e')}_{z_m} \right\} \Big/ \Delta\theta_e, \quad (6.2)$$

where $F_{H_-} - F_{z_m}$ is the longwave radiative divergence between the inversion height H_ and the aircraft measuring height z_m. Applying the selection described above, the number of entrainment velocities that we were able to determine reduced to 7. We estimate the error in each individually determined entrainment velocity between 50% and 80%, which results from the uncertainty in the jump across the inversion and the uncertainty in the fluxes of ozone and water vapor in the cloud layer. Therefore, the entrainment velocities presented in this section are merely a rough estimation of the order of magnitude rather than an accurate well-determined quantity.

The results are shown in Fig. 12. When we average

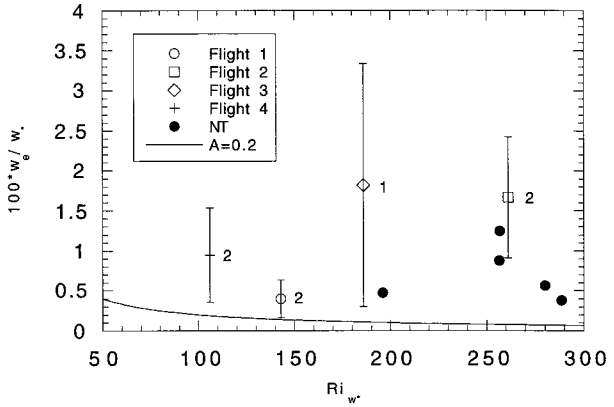

FIG. 12. Flux-derived entrainment velocities as a function of the convective Richardson number Ri_{w*} for Flights 1–4. The number of variables used is shown on the right of the mean entrainment velocity. Also plotted are aircraft-derived entrainment velocities from NT (Nicholls and Turton 1986) and a theoretical curve for the entrainment velocity for the dry convective boundary layer ($A = 0.2$). Symbols and line are according to the legend.

the calculated mean entrainment velocities for Flights 1–4, we find $\overline{w_e} = 0.9$ (± 0.5) cm s^{-1}. BAS calculated the mean entrainment velocity for the whole First Lagrangian (including Flight 5) from the ECMWF model and from a budget study, and found $\overline{w_e} = 0.9$ (± 0.5) cm s^{-1} and $\overline{w_e} = 1.0$ (± 0.4) cm s^{-1}, respectively. Their calculations and our results are in good agreement and are within measurement error. During Flight 3, three sets of two horizontal legs at about 2000-m altitude were flown within a total time interval of about 4.5 hours. These runs could be used to investigate the lidar data measured aboard the Electra aircraft to calculate the average cloud-top height because the minimum distance between the lidar and the cloud boundary should at least be 700 m. From the best fit line through the calculated cloud-top heights (H) as a function of time it was found that H increased at a rate of 0.6 (± 0.3) cm s^{-1}. Using $w_e = dH/dt - \overline{w}$, with $\overline{w} = -0.3$ (± 0.5) cm s^{-1} (BAS), the entrainment velocity from lidar measurements during Flight 3 is estimated $w_e = 1.0$ (± 0.6) cm s^{-1}, in good agreement with the ozone flux-derived entrainment rate 1.2 (± 1.0) cm s^{-1}. To compare our entrainment velocities with other aircraft-derived entrainment velocities, we also plotted results from Nicholls and Turton (1986), which are about the same order of magnitude as in Flights 2, 3, and 4. Lower entrainment velocities of about 0.3 cm s^{-1} were found in daytime stratocumulus cloud decks off the southern Californian coast by Kawa and Pearson (1989) derived from both ozone and total water fluxes. With typical cloud depths of 150–300 m these cloud layers were generally thinner than observed during the First Lagrangian, and every measurement was strongly influenced by solar absorption since, except for one flight, the aircraft flights took place around noon. For Flight 1, however, we also find a relatively small entrainment rate. Possibly, this may be caused by the two-layered cloud structure and the horizontal inhomogeneity since at many levels the cloud fraction was less than unity.

The line in Fig. 12 represents the entrainment velocity for the dry convective boundary layer according to (Nicholls and Turton 1986)

$$\frac{w_e}{w_*} = A\,\mathrm{Ri}_{w*}^{-1}, \qquad \left(\mathrm{Ri}_{w*} = \frac{gH}{\theta_v}\frac{\Delta\overline{\theta_v}}{w_*^2}\right), \qquad (6.3)$$

where Ri_{w*} is a Richardson number for convectively driven layers. Here A is constant and is about 0.2 for the dry convective atmospheric BL (Driedonks 1982). If the entrainment for cloudy boundary layer would scale as a function of the inverse Richardson number similar to Eq. (6.3), the entrainment velocity should increase relatively by a factor of 1.8 from Flight 2 to 4. The systematic larger values for the entrainment in a cloudy BL suggest that the entrainment is larger than in a dry convective boundary layer. Although we are aware of the large error in the flux-derived entrainment velocities, the results of Fig. 12 suggest that for Flights 2, 3, and 4 the entrainment velocity is about the same order of magnitude. Physically this means, using Eq. (5.3), that during Flight 4 there is an enhanced input of dry inversion air into the boundary layer relative to Flights 2 and 3 since the jump in the total water content during Flight 4 is larger than in the previous flights. Possibly, the enhanced entrainment of relatively warm and dry air is an important process for stimulating the breakup of the stratocumulus as observed during Flight 5.

7. Conclusions

Data from the First Lagrangian of ASTEX are analyzed. This Lagrangian experiment was undertaken over the Atlantic Ocean between 12 and 14 June 1992 in order to investigate the transition of stratocumulus to cumulus clouds. The U.K. MRF Hercules C-130 and NCAR Electra aircraft were used to take measurements in approximately the same air mass for about two days. Within this period four flights were made in stratocumulus cloud fields (Flights 1–4), whereas Flight 5 was flown in a field consisting of broken stratocumulus penetrated by cumulus from below. Cumulus clouds developing below the solid stratocumulus were also observed during Flights 3 and 4. Nevertheless, during these flights the dynamics were determined mainly by stratocumulus clouds. In this paper we discussed the mean state, cloud-top stability, and turbulence from the horizontal and porpoise aircraft legs.

During the first part of the Lagrangian the BL depth increased only slightly (30 m) between Flights 1 and 3. However, in the second part of the Lagrangian the BL height increased from about 770 to 1600 m as observed between Flights 4 and 5. During the five flights average wind velocities varied between 5 and 10 m s^{-1} from northerly directions. In all cases there was negligible

wind shear across the inversion. During the First Lagrangian, the SST increased from 16.8 (±0.5) to 21.1 (±0.3)°C. On Flight 1 the virtual potential temperature at the sea surface was lower than that of the BL and therefore was stably stratified. The mean BL temperature cooled between Flights 1 and 2, whereas the liquid water content probably increased as a result of the lowering of the saturated mixing ratio. In the free atmosphere the virtual potential temperature was nearly constant with time, suggesting that the warming due to large-scale subsidence and cooling by longwave radiative loss were approximately in equilibrium. In the cases where stratocumulus was observed, the total water content did not vary much, indicating that the surface input of moisture by turbulent surface fluxes, loss by drizzle, and drying by entrainment balanced each other.

We applied eddy correlation to determine the turbulent fluxes using a 31-sec running mean filter. We found that the buoyancy flux from the surface was positive but small during all flights except Flight 1. During this flight the surface buoyancy flux was slightly negative due to a stable surface stratification. In the stratocumulus-topped boundary layer maximum buoyancy fluxes were found near the cloud top, indicating the dominance of negatively buoyant downdrafts formed by longwave radiative cooling. During Flight 4, this buoyancy flux was found to be much larger than on the previous flights. Using Eq. (5.4) we showed that this was possibly due to the inversion stratification, which became less stable as a result of the warming of the BL due mainly to solar radiative absorption, surface warming, and increasing BL height by entrainment. During Flight 4, we found a larger negative total water jump that supports evaporative cooling when free atmosphere air is mixed into the boundary layer. We calculated the drizzle flux from the droplet spectra. From these measurements it was shown that only during Flight 3 a considerable amount of precipitation actually reached the surface; during Flights 2 and 4 the gradient in the drizzle flux suggested that there was considerable evaporation of droplets in the subcloud layer. Near the surface we found very small moisture fluxes. In the cloud layer a relative increase in the turbulent flux of total water was observed during Flight 4, which possibly reflects that during this flight more dry air could be entrained into the cloud layer as a result of a larger total water jump across the inversion.

The vertical velocity variances and TKE suggested that the BL was decoupled during Flights 4 and 5 since two local maxima were found in the subcloud and cloud layer. During Flight 4 the vertical velocity variance was significantly larger in the cloud layer than in the subcloud layer, which was also the case for Flight 1. The convection in these cloud layers was mainly driven from the cloud top because of a stable surface stratification (Flight 1) or decoupling of the cloud layer from the subcloud layer (Flight 4). During Flight 1 the skewness showed merely negative values, which reflect that negatively buoyant downdrafts dominated the convection. In contrast, during Flights 2 and 3 the vertical velocity variances scaled with the dry convective BL parameterization, as suggested by Lenschow et al. (1980). For these cases the buoyancy flux near the surface was of the same order of magnitude as near the cloud top possibly because entrainment warming could for a large part compensate for the longwave radiative cooling near the top of the cloud (Duynkerke et al. 1995); thus they were about equally important in generating TKE. Also, for Flights 2 and 3, the vertical velocity skewness showed very small positive values in the cloud layer, suggesting that updrafts and downdrafts are equally important. During Flights 3–5 the positive values of skewness near the surface illustrated that the unstable surface stratification became more important in generating convection. On Flight 5 the skewness showed a maximum of about 2 in the middle of the cloud layer as a result of intensive cumulus convection. Although cumulus clouds were observed to penetrate the inversion during Flight 4, the low skewness values in the upper part of the cloud layer suggested that they were not dominating the vertical convection but are probably as important as the convection driven from the top.

From the porpoise runs we determined the cloud-top jumps of equivalent potential temperature and total water content. The scatter in the results on one flight was considerable and was probably due to large-scale horizontal variations and inhomogeneities above the inversion. We have discussed stability criteria of Randall (1980), Deardorff (1980), MacVean and Mason (1990), and Duynkerke (1993). Flight 4 was unstable according to Randall (1980) and Deardorff (1980) but stable to the curves suggested by MacVean and Mason (1990) and Duynkerke (1993), although the stability was observed to decrease from Flight 2 to 4 with respect to the latter two criteria. This was caused by enlarging jumps in the total water content and a larger negative equivalent potential temperature jump. These changes in jumps were due mainly to a warming of the cloud layer by the absorption of solar radiation, warming by increasing SST, and BL growth by entrainment. The observed jumps seem to fit on the line $\Delta\theta_l = 5$ K, which contrasts with the cases summarized by Kuo and Schubert (1988), who found that the jumps were approximately arranged along the line $\Delta\theta_l = 9$ K. This difference is mainly due to a smaller potential temperature jump during the First Lagrangian than in the cases summarized by Kuo and Schubert (1988). From the turbulent fluxes of ozone, total water, and equivalent potential temperature we derived entrainment velocities. The mean entrainment velocity, $\overline{w}_e = 0.9$ (±0.5) cm s^{-1}, was in good agreement with results from the ECMWF and a budget study presented by Bretherton et al. (1995). They were also of the same order of magnitude as aircraft-derived entrainment rates found by Nicholls and Turton (1986). Their results, and the entrainment rates found during the First Lagrangian, are

significantly larger than entrainment rates predicted for the dry convective boundary layer (Driedonks 1982). However, for daytime stratocumulus layers smaller entrainment rates of about 0.3 cm s^{-1} were calculated by Kawa and Pearson (1989).

Because the total water flux near the top of the cloud was found to increase from Flight 2 to 4, it is suggested that the process of enhanced entrainment of dry air from above the inversion and subsequent mixing into the stratocumulus cloud layer might be an important mechanism in stimulating the cloud to break up, as was observed during Flight 5. Furthermore, besides entrainment drying, decoupling of the cloud layer during Flight 4 prevents mixing of water vapor from the surface into the cloud layer, thereby cutting off the main source for cloud maintenance. Since Flight 4 ended around sunset, the effect of solar absorption on the dissipation of the stratocumulus cloud can be neglected.

Acknowledgments. The investigations were in part supported by the Netherlands Geosciences Foundation (GOA) with financial aid (Grant 750.295.03A) from the Netherlands Organization for Scientific Research (NWO). Dr. Doug Johnson and Dr. Gill Martin of the U.K. Meteorological Research Flight and Dr. D. Lenschow of NCAR kindly provided the aircraft data, and Dr. Ken Davis (NCAR) supplied the lidar data. The authors also would like to thank Piet Jonker for providing the computer software and Dr. Bert Holtslag for critically reading the manuscript.

REFERENCES

Albrecht, B. A., C. S. Bretherton, D. W. Johnson, W. H. Schubert, and A. S. Frisch, 1994: The Atlantic Stratocumulus Transition Experiment—ASTEX. *Bull. Amer. Meteor. Soc.,* **76,** 889–904.

Bretherton, C. S., and R. Pincus, 1995: Cloudiness and marine boundary layer dynamics in the ASTEX Lagrangian experiments. Part I: Synoptic setting and vertical structure. *J. Atmos. Sci.,* **52,** 2707–2723.

——, P. Austin, and S. T. Siems, 1995: Cloudiness and marine boundary layer dynamics in the ASTEX Lagrangian experiments. Part II: Cloudiness, drizzle, surface fluxes, and entrainment. *J. Atmos. Sci.,* **52,** 2724–2735.

Brost, R. A., D. H. Lenschow, and J. C. Wyngaard, 1982a: Marine stratocumulus layers. Part I: Mean conditions. *J. Atmos. Sci.,* **39,** 800–817.

——, J. C. Wyngaard, and D. H. Lenschow, 1982b: Marine stratocumulus layers. Part II: Turbulence budgets. *J. Atmos. Sci.,* **39,** 818–836.

Caughey, S. J., and M. Kitchen, 1984: Simultaneous measurements of the turbulent and microphysical structure of nocturnal stratocumulus cloud. *Quart. J. Roy. Meteor. Soc.,* **110,** 13–34.

——, B. A. Crease, and W. T. Roach, 1982: A field study of nocturnal stratocumulus: II. Turbulence structure and entrainment. *Quart. J. Roy. Meteor. Soc.,* **108,** 125–144.

Cuijpers, J. W. M., P. G. Duynkerke, and F. T. M. Nieuwstadt, 1996: Analyses of variance and flux budgets in cumulus-topped boundary layers. *Atmos. Res.,* **40,** 307–338.

Deardorff, J. W., 1980: Cloud-top entrainment instability. *J. Atmos. Sci.,* **37,** 131–147.

de Roode, S. R., and P. G. Duynkerke, 1996: Dynamics of cumulus rising into stratocumulus as observed during the first ''Lagrangian'' experiment of ASTEX. *Quart. J. Roy. Meteor. Soc.,* **122,** 1597–1623.

Driedonks, A. G. M., 1982: Models and observations of the growth of the atmospheric boundary layer. *Bound.-Layer Meteor.,* **23,** 283–306.

Duynkerke, P. G., 1993: The stability of cloud top with regard to entrainment: Amendment of the theory of cloud-top entrainment instability. *J. Atmos. Sci.,* **50,** 495–502.

——, H. Q. Zhang, and P. J. Jonker, 1995: Microphysical and turbulent structure of nocturnal stratocumulus as observed during ASTEX. *J. Atmos. Sci.,* **52,** 2763–2777.

Hignett, P., 1991: Observations of diurnal variation in a cloud-capped marine boundary layer. *J. Atmos. Sci.,* **48,** 1474–1482.

Kawa, S. R., and R. Pearson Jr., 1989: An observational study of stratocumulus entrainment and thermodynamics. *J. Atmos. Sci.,* **46,** 2649–2661.

Kuo, H., and W. H. Schubert, 1988: Stability of cloud-topped boundary layers. *Quart. J. Roy. Meteor. Soc.,* **114,** 887–916.

Lenschow, D. H., J. C. Wyngaard, and W. T. Pennell, 1980: Mean-field and second-moment budgets in a baroclinic, convective boundary layer. *J. Atmos. Sci.,* **37,** 1313–1326.

——, J. Mann, and L. Kristensen, 1994: How long is long enough when measuring fluxes and other turbulence statistics? *J. Atmos. Oceanic Technol.,* **11,** 661–673.

Lilly, D. K., 1968: Models of cloud-topped mixed layers under a strong inversion. *Quart. J. Roy. Meteor. Soc.,* **94,** 292–309.

MacVean, M. K., and P. J. Mason, 1990: Cloud-top entrainment instability through small-scale mixing and its parameterization in numerical models. *J. Atmos. Sci.,* **47,** 1012–1030.

Martin, G. M., D. W. Johnson, D. P. Rogers, P. R. Jonas, P. Minnis, and D. A. Hegg, 1995: Observations of the interaction between cumulus clouds and warm stratocumulus clouds in the marine boundary layer during ASTEX. *J. Atmos. Sci.,* **52,** 2902–2922.

Nicholls, S., 1984: The dynamics of stratocumulus: Aircraft observations and comparisons with a mixed layer model. *Quart. J. Roy. Meteor. Soc.,* **110,** 783–820.

——, 1989: The structure of radiatively driven convection in stratocumulus. *Quart. J. Roy. Meteor. Soc.,* **115,** 487–511.

——, and J. Leighton, 1986: An observation study of the structure of stratiform cloud sheets: Part I. Structure. *Quart. J. Roy. Meteor. Soc.,* **112,** 431–460.

——, and J. D. Turton, 1986: An observational study of the structure of stratiform cloud sheets: Part II. Entrainment. *Quart. J. Roy. Meteor. Soc.,* **112,** 461–480.

Randall, D. A., 1980: Conditional instability of the first kind upside down. *J. Atmos. Sci.,* **37,** 125–130.

Rogers, D. P., X. Yang, P. M. Norris, D. W. Johnson, G. M. Martin, C. A. Friehe, and B. W. Berger, 1995: Diurnal evolution of the cloud-topped marine boundary layer. Part I: Nocturnal stratocumulus development. *J. Atmos. Sci.,* **52,** 2953–2966.

Rogers, R. R., 1979: *A Short Course in Cloud Physics.* 2d ed. Pergamon Press, 235 pp.

Siems, S. T., and C. S. Bretherton, 1992: A numerical investigation of cloud-top entrainment instability and related experiments. *Quart. J. Roy. Meteor. Soc.,* **118,** 787–818.

Smith, S. A., and P. R. Jonas, 1995: Observations of the turbulent fluxes in fields of cumulus clouds. *Quart. J. Roy. Meteor. Soc.,* **121,** 1185–1208.

Wang, Q., and D. H. Lenschow, 1995: An observational study of the role of penetrating cumulus in a marine stratocumulus-topped boundary layer. *J. Atmos. Sci.,* **52,** 2778–2787.

Young, G. S., 1987: Mixed layer spectra from aircraft measurements. *J. Atmos. Sci.,* **44,** 1251–1256.